Critical Role of a Sheath Phosphorylation Site On the Assembly and Function of an Atypical Type VI Secretion System

Jason Ziveri, Cerina Chhuon, Anne Jamet, Héloïse Rytter, Guénolé Prigent, Fabiola Tros, Monique Barel, Mathieu Coureuil, Claire Lays, Thomas Henry, et al.

Critical Role of a Sheath Phosphorylation Site On the Assembly and Function of An Atypical Type VI Secretion System

Authors

Jason Ziveri, Cerina Chhuon, Anne Jamet, Héloïse Rytter, Guénolé Prigent, Fabiola Tros, Monique Barel, Mathieu Coureuil, Claire Lays, Thomas Henry, Nicholas H. Keep, Ida Chiara Guerrera, and Alain Charbit

Correspondence

alain.charbit@inserm.fr;
chiara.guerrera@inserm.fr

Graphical Abstract

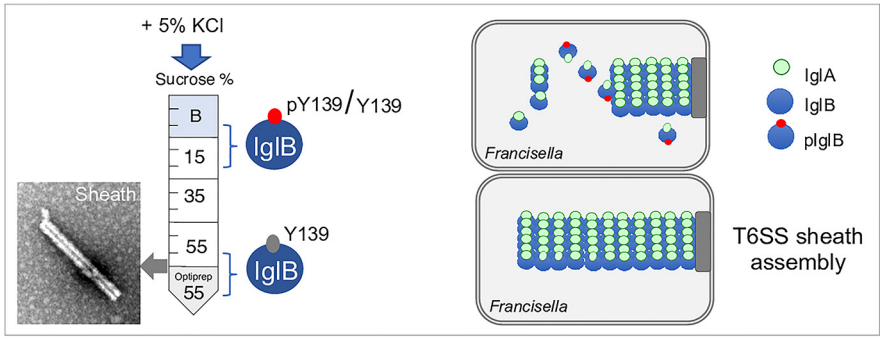

In Brief

KCl stimulation triggers assembly of the Francisella T6SS in culture. Differential whole cell proteomics reveals that the amounts of the T6SS proteins remain unchanged upon KCl stimulation. A phosphoproteomic analysis identifies a phosphorylation on the T6SS sheath, at site Y139 of IglB. Our data demonstrate that site Y139 of IglB plays a critical role in T6SS biogenesis, providing novel mechanistic insight into the role of sheath phosphorylation in T6SS biogenesis.

Highlights

- Phosphorylation on Y139 of the sheath protein IglB of *Francisella*.
- IglB substitutions Y139A, Y139D or Y139E prevent T6SS formation.
- Y139F substitution delays but does not abolish phagosomal escape in macrophages.
- Insight into the role of sheath phosphorylation in T6SS biogenesis.

Ziveri et al., 2019, Molecular & Cellular Proteomics *18*, 2418–2432
December 2019
https://doi.org/10.1074/mcp.RA119.001532

Critical Role of a Sheath Phosphorylation Site On the Assembly and Function of an Atypical Type VI Secretion System*[S]

Jason Ziveri‡§§, Cerina Chhuon§§§, Anne Jamet‡§§, Héloïse Rytter‡§§, Guénolé Prigent‡§§, Fabiola Tros‡§§, Monique Barel‡§§, Mathieu Coureuil‡§§, Claire Lays‖, Thomas Henry‖, Nicholas H. Keep¶, Ida Chiara Guerrera§‡‡§§, and Alain Charbit‡**§§

The bacterial pathogen *Francisella tularensis* possesses a noncanonical type VI secretion system (T6SS) that is required for phagosomal escape in infected macrophages. KCl stimulation has been previously used to trigger assembly and secretion of the T6SS in culture. By differential proteomics, we found here that the amounts of the T6SS proteins remained unchanged upon KCl stimulation, suggesting involvement of post-translational modifications in T6SS assembly. A phosphoproteomic analysis indeed identified a unique phosphorylation site on IglB, a key component of the T6SS sheath. Substitutions of Y139 with alanine or phosphomimetics prevented T6SS formation and abolished phagosomal escape whereas substitution with phenylalanine delayed but did not abolish phagosomal escape in J774–1 macrophages. Altogether our data demonstrated that the Y139 site of IglB plays a critical role in T6SS biogenesis, suggesting that sheath phosphorylation could participate to T6SS dynamics.

Data are available via ProteomeXchange with identifier PXD013619; and on MS-Viewer, key lkaqkllxwx ***Molecular & Cellular Proteomics 18: 2418–2432, 2019. DOI: 10.1074/mcp.RA119.001532.***

Francisella tularensis is the causative agent of the zoonotic disease tularemia (1–4). Four major subspecies (subsp)[1] of *F. tularensis* are currently listed to cause a fulminant disease in mice that is like tularemia in human (5, 6). Although the subsp *novicida* (also called *F. novicida) is* rarely pathogenic in human, its genome shares a high degree of nucleotide sequence conservation with the human pathogenic species and is thus widely used as a model organism (7–9).

This facultative intracellular pathogen can infect a variety of different cell types but, *in vivo*, is thought to replicate and disseminate mainly in phagocytes (10). *Francisella* phagosomal escape occurs as early as 30 min post-infection (11). Several factors controlling *Francisella* phagosomal escape and cytosolic multiplication have been already characterized (2, 12–16). Notably, the crucial role of a 30-kb locus in *Francisella* virulence (supplemental Fig. S1), designated FPI for "Francisella pathogenicity island" (17), has been extensively documented (18). Of note, the FPI is duplicated in three subspecies of *F. tularensis* (subsps *holarctica*, *mediasiatica*, and *tularensis*), but is present in a single copy in *F. novicida* and *F. philomiragia*. The FPI encodes a Type VI secretion system (T6SS) that is essential to promote bacterial phagosomal escape and access to the cytosolic replication niche (19–21). Whereas the transcriptional regulation of the FPI locus has been deeply characterized (22), the molecular mechanisms triggering T6SS assembly and contraction remain largely unknown. Bioinformatic analyses have divided bacterial T6SS in three phylogenetically distinct subtypes (designated T6SSi-iii) (23). Whereas most of the well-characterized T6SS belong to the T6SSi (including in *P. areruginosa* and *V. cholerae*), *Francisella* is currently the only bacterium to possess a T6SSii (24) known to be exclusively involved in the intracellular life cycle of the pathogen.

The FPI encodes, in addition to the T6SS components, a number of proteins of unknown functions some of which (such as IglF,PdpC or PdpD) have been proposed or demonstrated to be T6SS effectors (8, 25).

Our current knowledge of the structure and functional assembly of the *Francisella* T6SS are mainly based on recent

From the ‡Université Paris Descartes, Sorbonne Paris Cité, INSERM U1151-CNRS UMR 8253, Institut Necker-Enfants Malades. Team 7: Pathogenesis of Systemic Infections, Paris 75015, France; §Plateforme protéomique 3P5-Necker, Université Paris Descartes - Structure Fédérative de Recherche Necker, INSERM US24/CNRS UMS3633, Paris 75015, France; ¶Crystallography, Institute for Structural and Molecular Biology, Department of Biological Sciences Birkbeck, University of London, United Kingdom; ‖CIRI, Centre International de Recherche en Infectiologie, Université Lyon, Inserm, U1111, University Claude Bernard Lyon 1, CNRS, UMR5308, École Normale Supérieure de Lyon, Labex Ecofect, Eco-evolutionary dynamics of infectious diseases, F-69007, LYON, France

Received April 29, 2019, and in revised form, September 3, 2019

Published, MCP Papers in Press, October 2, 2019, DOI 10.1074/mcp.RA119.001532

cryo-electron microscopy data (26, 27) and structural homologies with other members of the T6SSi (26, 27) and references therein). It has been proposed that T6SS resembles a syringe: the tube comprised of IglC subunits (Hcp homologue) that form hexameric rings fits within the cavity of the IglA/IglB sheath (TssB/C in *Pseudomonas*, VipA/B in *Vibrio*), contraction of the sheath results in the ejection of the Hcp tube, together with effector proteins located within the tube and on top of the tip of the tube (28).

Formation of the contracted *Francisella* T6SS can be mimicked *in vitro* by high K^+ concentration (26). Yet, the molecular relay for this environmental cue remains uncharacterized. To understand the mechanisms underlying this KCl-induced T6SS production, we performed a global proteomic analysis on KCl-induced and noninduced bacteria. We found that the relative amounts of most FPI proteins were not increased upon KCl stimulation that suggested the possible implication of a post-translational control of T6SS polymerization.

Post-translational modifications (PTMs) constitute a common mechanism that eukaryotic cells employ to polymerize biomolecules. However, in bacteria, polymerization mechanisms are more generally driven by gene expression regulation than by PTMs. Although T6SS sheath polymerization had never been shown to involve any PTM, we hypothesized that protein phosphorylation might occur in *Francisella* and contribute to the dynamics of T6SS assembly-disassembly. By using state-of-the art mass spectrometry analyses, we indeed identified more than one hundred peptides bearing serine/threonine/or tyrosine phosphorylated residues in the proteome of *F. novicida.* One peptide, corresponding to a phosphorylation of IglB on tyrosine 139 (Y139), particularly attracted our attention. The data presented here reveal that the unique phosphorylatable site of IglB is essential for the proper activity of this noncanonical T6SS. Functional implications are discussed.

EXPERIMENTAL PROCEDURES

Experimental Design and Statistical Rationale—The (phospho)proteomics data is derived from 3 sets of samples prepared and analyzed by LC-MS/MS for a total of 60 runs performed with 120 min gradient for proteome and 180 min gradient for phosphoproteome measurements on a Q Exactive Plus mass spectrometer. For the proteome data we performed 24 runs for 8 samples (four biological replicates per condition, each run in three technical replicates). For the phosphoproteome data we also performed 24 runs for 8 samples, (four biological replicates per condition, each run in three technical replicates). For the heavy and light sucrose fractions we ran 12 samples in one simple replicate for qualitative analysis. Raw data was processed by MaxQuant software (version 1.5.3.30) as described below. Statistical analysis was performed with Perseus (version 1.6.2.3). For proteome analysis we used *t* test, and filtered using S0 = 0.5, FDR = 0.01 (for class B proteins) and the outer volcano using S0 = 0.5, FDR = 0.001 (class A proteins). For phosphoproteomics analysis we used used *t* test S0 = 0.1, FDR = 0.05. For functional class annotation, COG and EggNog databases were integrated in Perseus.

For detailed description of data analysis of each experiment see MS data analysis in the section methods.

For all other experiments: All biological assays were performed in three biological and technical replicates, so that appropriate statistical analysis could be performed. Statistical analysis was performed with two tailed unpaired *t* test in GraphPad Prism. p values < 0.05 were considered statistically significant, with * for $p < 0.05$, ** for $p < 0.01$, *** for $p < 0.001$ and **** for $p < 0.0001$. In each experiment, separate controls were included. Images of experiments and Western blotting were quantified using ImageJ software.

Strains and Culture Conditions—All strains used in this study are derived from *F. novicida* U112 as described in supplemental Table S1. Strains were grown at 37 °C on pre-made chocolate agar PolyViteX plates (BioMerieux), Schaedler K3 or Chemically Defined Medium (CDM). The CDM used for *F. novicida* corresponds to standard CDM (29) without threonine and valine (30). For growth condition determination, bacterial strains were inoculated in the appropriate medium at an initial OD_{600} of 0.05 from an overnight culture in Schaedler K3 medium.

T6SS Purification—T6SS were prepared essentially as described in (26). Briefly, wild-type *F. novicida* was grown to late exponential phase in Schaedler K3 containing 5% KCl; pelleted by centrifugation and lysed with lysozyme and 1% TritonX-100 detergent in 20 mM Tris HCl, (pH 7.8) with 1 mM EDTA, protease inhibitor mixture and benzonase nuclease. The lysate was centrifuged 3 times at 15,000 × *g* for 30 min at 4 °C to pellet bacterial debris, and the supernatant was layered onto a 10–55% sucrose gradient overlying a 55% Optiprep cushion and centrifuged at 100,000 × *g* for 18 h. Fractions were collected and examined by transmission electron microscopy (TEM) after negative staining. Briefly, fractions were fixed in 3% paraformaldehyde. Electron microscopy grids were placed on a drop of this suspension and rinsed. The negative contrast was obtained by treating the grids with 2% uranyl acetate for 5 min. The Formvar-coated grids were then observed with a JEOL 1011 transmission electron microscope (tungsten filament) at the Institut Cochin (Paris, France). The sheath-like structures sedimented to just below the 55% sucrose/Optiprep interface

Proteomic and Phosphoproteomic Analyses

Reagents and Chemicals—For protein digestion, dithiothreitol, iodoacetamide and ammonium bicarbonate were purchased from Sigma-Aldrich (St Louis, MO). For phosphopeptide enrichment and LC-MS/MS analysis, trifluoroacetic acid (TFA), formic acid, acetonitrile and HPLC-grade water were purchased from Fisher Scientific (Pittsburgh, PA) at the highest purity grade.

Protein Digestion—For proteomic analysis, *F. novicida* was analyzed in three independent biological replicates. Protein concentration was determined by DC assay (Bio-Rad, CA) according to the manufacturer's instructions. An estimated 1.2 mg of proteins for each biological replicate were digested following a FASP protocol (31) slightly modified. Briefly, proteins were reduced using 100 mM dithiothreitol in 50 mM ammonium bicarbonate for 1 h at 60 °C. Proteins were then split into four samples of 300 μg and applied on 30 kDa MWCO centrifugal filter units (Microcon, Millipore, Germany, Cat No

[1] The abbreviations used are: Subsp, Subspecies; T6SS, Type VI secretion system; BMDM, Bone marrow-derived macrophages; CDM, Chemically defined medium; CFU, Colony forming unit; CI, Competition index; DMEM, Dubelcco's modified eagle medium; $Ti0_2$, Titanium dioxide; ASC, Apoptosis-associated speck-like protein containing a CARD; FCP, *Francisella*-containing phagosome; FPI, *Francisella* pathogenicity Island; KEGG, Kyoto encyclopedia of genes and genomes; LAMP, Lysosomal associated membrane protein; LC-MS/MS, Liquid chromatography coupled to tandem mass spectrometry; LFQ, Label free quantification; FDR, False discovery rate; MOI, Multiplicity of infection; OD, Optical density; TSB, Tryptic soy broth.

MRCF0R030). Samples were mixed with 200 μl of 8 M urea in 50 mM ammonium bicarbonate (UA buffer) and centrifuged for 20 min at 15,000 × *g*. Filters were washed with 200 μl of UA buffer. Proteins were alkylated for 30min by incubation in the dark at room temperature with 100 μl of 50 mM iodoacetamide in UA buffer. Filters were then washed twice with 100 μl of UA buffer (15,000 × *g* for 15 min) followed by two washes with 100 μl of 50 mM ammonium bicarbonate (15,000 × *g* for 10 min). Finally, sequencing grade modified trypsin (Promega, WI) was added to digest the proteins in 1:50 ratio for 16 h at 37 °C. Peptides were collected by centrifugation at 15,000 × *g* for 10 min followed by one wash with 50 mM ammonium bicarbonate and vacuum dried.

Phosphopeptides Enrichment by Titanium Dioxide (TiO_2) and Phosphopeptides Purification by Graphite Carbon (GC).—Phosphopeptide enrichment was carried out using a Titansphere TiO_2 Spin tip (3 mg/200 μl, Titansphere PHOS-TiO, GL Sciences Inc, Japan) an estimated 1.2 mg of digested proteins for each biological replicate. Briefly, the TiO_2 Spin tips were conditioned with 20 μl of solution A (80% acetonitrile, 0,1% TFA), centrifuged at 3000 × *g* for 2min and equilibrated with 20 μl of solution B (75% acetonitrile, 0,075% TFA, 25% lactic acid) followed by centrifugation at 3000 × *g* for 2 min. Peptides were resuspended in 10 μl of 2% TFA, mixed with 100 μl of solution B and centrifuged at 1000 × *g* for 10min. Sample was applied back to the TiO_2 Spin tips two more times to increase the adsorption of the phosphopeptides to the TiO_2. Spin tips were washed with, sequentially, 20 μl of solution B and two times with 20 μl of solution A. Phosphopeptides were eluted by the sequential addition of 50 μl of 5% NH_4OH and 50 μl of 5% pyrrolidine. Centrifugation was carried out at 1000 × *g* for 5 min.

Phosphopeptides were further purified using GC Spin tips (GL-Tip, Titansphere, GL Sciences Inc, Japan). Briefly, the GC Spin tips were conditioned with 20 μl of solution A, centrifuged at 3000 × *g* for 2 min and equilibrated with 20 μl of solution C (0,1% TFA in HPLC-grade water) followed by centrifugation at 3000 × *g* for 2 min. Eluted phosphopeptides from the TiO_2 Spin tips were added to the GC Spin tips and centrifuged at 1,000 × *g* for 5 min. GC Spin tips were washed with 20 μl of solution C. Phosphopeptides were eluted with 70 μl of solution A (1000 × *g* for 3 min) and vacuum dried.

nanoLC-MS/MS Protein Identification and Quantification—Samples were resuspended in 12 μl of 0.1% TFA in HPLC-grade water. For each run, 5 μl was injected in a nanoRSLC-Q Exactive PLUS (RSLC Ultimate 3000, Thermo Scientific, MA). Phosphopeptides were loaded onto a μ-precolumn (Acclaim PepMap 100 C18, cartridge, 300 μm i.d.×5 mm, 5 μm, Thermo Scientific, MA) and were separated on a 50 cm reversed-phase liquid chromatographic column (0.075 mm ID, Acclaim PepMap 100, C18, 2 μm, Thermo Scientific, MA). Chromatography solvents were (A) 0.1% formic acid in water, and (B) 80% acetonitrile, 0.08% formic acid. Phosphopeptides were eluted from the column with the following gradient 5% to 40% B (180 min), 40% to 80% (6 min). At 181 min, the gradient returned to 5% to re-equilibrate the column for 20 min before the next injection. Two blanks were run between each sample to prevent sample carryover.

Phosphopeptides eluting from the column were analyzed by data dependent MS/MS, using top-8 acquisition method. Phosphopeptides were fragmented using higher-energy collisional dissociation (HCD). Briefly, the instrument settings were as follows: resolution was set to 70,000 for MS scans and 17,500 for the data dependent MS/MS scans to increase speed. The MS AGC target was set to 1×10^6 counts with maximum injection time set to 250 ms, whereas MS/MS AGC target was set to 2×10^5 with maximum injection time set to 250 ms. The MS scan range was from 400 to 1.800 *m/z*. MS and MS/MS scans were recorded in profile mode. Dynamic exclusion was set to 30 s.

For proteomic analysis, peptides were eluted from the column with the following gradient 5% to 40% B (120 min), 40% to 80% (6 min). At 127 min, the gradient returned to 5% to re-equilibrate the column for 20 min before the next injection. Peptides eluting from the column were analyzed by data dependent MS/MS, using the top-10 acquisition method. Peptides were fragmented using higher-energy collisional dissociation (HCD). Briefly, the instrument settings were as follows: resolution was set to 70,000 for MS scans and 17,500 for the data dependent MS/MS scans to increase speed. The MS AGC target was set to 3.106 counts with maximum injection time set to 60 ms, whereas MS/MS AGC target was set to 1.105 with maximum injection time set to 60 ms. The MS scan range was from 400 to 2000 *m/z*. Dynamic exclusion was set to 30 s duration.

Data Processing Following nanoLC-MS/MS Acquisition—The MS files were processed with the MaxQuant software version 1.5.3.30 and searched with Andromeda search engine against the UniProtKB/Swiss-Prot *F. novicida* database (release 28–04-2014, 1719 entries). To search parent mass and fragment ions, we set an initial mass deviation of 4.5 ppm and 0.5 Da respectively. The minimum peptide length was set to 7 amino acids and strict specificity for trypsin cleavage was required, allowing up to two missed cleavage sites. Carbamidomethylation (Cys) was set as fixed modification, whereas oxidation (Met), N-term acetylation and phosphorylation (Ser, Thr, Tyr) were set as variable modifications (only for phosphoproteomics analysis). The match between runs option was enabled with a match time window of 0.7 min and an alignment time window of 20 min. The false discovery rates (FDRs) at the protein and peptide level were set to 1%. Scores were calculated in MaxQuant as described previously (32). The reverse and common contaminants hits were removed from MaxQuant output.

The phosphopeptides output table and the corresponding logarithmic intensities were used for phosphopeptide analysis. The phosphopeptide table was expanded to separate individual phosphosites, and we kept all sites identified in at least three out of four replicates in at least one groupe (no KCl *versus* KCl). Missing values were imputed using width = 0.2 and down-shift = 3. We represented on a heatmap the significantly altered phosphosites (*t* test S0 = 0.1, FDR = 0.05).

The proteingroups output table was used for total proteome analysis, we kept only proteins identified in all four replicates in at least one group (noKCl *versus* KCl). Missing values were imputed using width = 0.3 and down-shift = 2.5. For volcano plot we used *t* test, S0 = 0.5, FDR = 0.01 (for class B proteins) and the outer volcano using S0 = 0.5, FDR = 0.001 (class A proteins).

Construction of a ΔiglB Deletion Mutant—We inactivated the gene *iglB* in *F. novicida* (*FTN_1323*) by allelic replacement, resulting in the deletion of the entire gene (4 first codons and 7 last codons were conserved). We constructed a recombinant PCR product containing the upstream region of the gene *iglB* (*iglB*-UP), a kanamycin resistance cassette (*nptII* gene fused with *pGro* promoter) and the downstream region of the gene *iglB* (*iglB*-DN) by overlap PCR. Primers *iglB* upstream FW (p1) and *iglB* upstream (spl_K7) RV (p2) amplified the 689 bp region upstream of position +3 of the *iglB* coding sequence (*iglB*-UP), primers *pGro* FW (p3) and *nptII* RV (p4) amplified the 1091 bp kanamycin resistance cassette (*nptII* gene fused with *pGro* promoter); and primers *iglB* downstream (spl_K7) FW (p5) and *iglB* downstream RV (p6) amplified the 622 bp region downstream of the position +1520 of the *iglB* gene coding sequence (*iglB*-DN). Primers p2 and p5 have an overlapping sequence of 12 nucleotides with primers p3 and p4 respectively resulting in fusion of *iglB*-UP and *iglB*-DN with the cassette after cross-over PCR (supplemental Table S2). All single fragment PCR reactions were realized using Phusion High-Fidelity DNA Polymerase (ThermoScientific) and PCR products were purified using NucleoSpin® Gel and PCR Clean-up kit (Macherey-Nagel). Overlap PCRs were carried out using 100 ng of each purified PCR

products and the resulting fragment of interest was purified from agarose gel. This fragment was then directly used to transform wild type *F. novicida* by chemical transformation (30). Recombinant bacteria were isolated on Chocolate agar plates containing kanamycin (10 μg ml^{-1}). The mutant strains were checked for loss of the wild type gene by PCR product direct sequencing (GATC-biotech) using appropriate primers.

Functional Complementation—The Δ*iglB* mutant strain was transformed with the recombinant pKK214-derived plasmids (pKK-*iglBY139A*$_{cp}$, pKK-*iglBY139F*$_{cp}$, pKK-*iglBY139D*$_{cp}$ and pKK-*iglBY139E*$_{cp}$) described below (supplemental Table S1). Primers pGroFW and pGro RV amplified the 328 bp of the *pGro* promoter; primers *iglB* FW/and *iglB*[PstI] RV amplified the 1,534 bp *iglB* gene from U112. PCR products were purified and SmaI (*pGro* promoter) or PstI (*iglB*) digested in presence of FastAP Thermosensitive Alkaline Phosphatase (ThermoScientific) to avoid self-ligation. Mixtures of *pGro* promoter and fragments of the genes of interest were then incubated with T4 DNA Ligase (New England Biolabs) to allow blunt end ligation and fragments were then cloned in pKK214 vector after SmaI/PstI double digest and transformed in *E. coli* TOP10. Recombinant plasmid pKK-*iglB*$_{cp}$ was purified and directly used for chemical transformation in *F. novicida* Δ*iglB* (30). Recombinant colonies were selected on Chocolate agar plates containing tetracycline (5 μg ml^{-1}) and kanamycin (10 μg ml^{-1}).

For site-directed mutagenesis of *iglB* gene, we used plasmid pKK-*iglB*$_{cp.}$ The recombinant plasmids pKK-*iglBY139A*$_{cp}$, pKK-*iglBY139F*$_{cp}$, pKK-*iglBY139D*$_{cp}$ and pKK-*iglBY139E*$_{cp}$ were constructed using the primer pairs iglB (Y/A, Y/F,Y/D, or Y/E) FW and iglB RV (supplemental Table S2). The three first bases of primers iglB FW were modified to change Tyr139 to Ala, Phe, Asp or Glu. PCR products were purified, phosphorylated by the T4 Polynucleotide Kinase and then incubated with T4 DNA Ligase (New England Biolabs) and transformed in *E. coli* TOP10. Recombinant plasmids were purified and directly used for chemical transformation in *F. novicida* Δ*iglB*, as described previously (30). Recombinant colonies were selected on Chocolate agar plates containing tetracycline (5 μg ml^{-1}) and kanamycin (10 μg ml^{-1}).

Gfp-expressing F. novicida—The Δ*iglB* mutant strain was transformed with the recombinant plasmids pKK-GFP-*iglBWT*$_{cp}$ and pKK-GFP-*iglBY139F*$_{cp,}$ derived from pKK214-GFP (33). Primers pGroFW and *iglB*RV (supplemental Table S2) amplified the 1,870 bp of the *pGro-iglB* from the pKK-*iglBWT*$_{cp}$ and pKK-*iglBY139F*$_{cp}$. PCR products were purified and digested with SmaI and the *pGro-iglB WT* and *pGro-iglB Y139F* fragments were then incubated with T4 DNA Ligase (New England Biolabs) to allow blunt end ligation and fragments were then cloned in the unique SmaI site of pKK214-(GFP) vector and transformed in *E. coli* TOP10. Recombinant plasmid pKK-(GFP)-*iglBWT*$_{cp}$ and pKK-(GFP)-*iglBY139F*$_{cp}$ were purified and directly used for chemical transformation in *F. novicida* Δ*iglB* (30). Recombinant colonies were selected on Chocolate agar plates containing tetracycline (5 μg ml^{-1}) and kanamycin (10 μg ml^{-1}).

Immunodetection—Antibodies to IglA, IglB and IglC were obtained through the NIH Biodefense and Emerging Infections (BEI) Research Resources Repository, NIAID, NIH.

Immunoblotting Analysis—Protein lysates for immunoblotting were prepared by using Laemmli sample buffer. Protein lysates corresponding to equal OD_{600} were loaded on 12% Bis/Tris gels (Invitrogen), and run in TGS buffer. Primary antibodies (anti-IglA or anti-IglB) were used at final dilution of 1:2000. Secondary horseradish peroxidase (HRP)-conjugated goat anti-mouse antibody (Santa Cruz Biotechnology, CA) or (HRP)-conjugated goat anti-rabbit antibody and the enhanced Chemiluminescence system (ECL) (Amersham Biosciences, Uppsala, Sweden) were used as previously described (34).

Co-immunoprecipitations—Wild-type *F. novicida* was grown to late exponential phase in Schaedler K3; collected by centrifugation and lysed with lysozyme and 1% TritonX-100 detergent in 20 mM Tris HCl, (pH 7.8) with 1 mM EDTA, protease inhibitor mixture and benzonase nuclease. The lysate was centrifuged at 15,000 g for 15 min at 4 °C to pellet bacterial debris. Monoclonal anti-IglB antibody was incubated 40 min with Dynabeads protein G (Invitrogen) and the complex was incubated at room temperature with the bacterial lysate for 1 h. After washing, the complex was loaded on 12% Bis/Tris gels (Invitrogen), and run in TGS buffer.

Cell Cultures and Cell Infection Experiments—J774A.1 (ATCC® TIB-67™) cells were propagated in Dulbecco's Modified Eagle's Medium (DMEM, PAA), containing 10% fetal bovine serum (FBS, PAA) unless otherwise stated. The day before infection, ~2 × 10^5 eukaryotic cells per well were seeded in 12-well cell tissue plates and bacterial strains were grown overnight in 5 ml of Schaedler K3 at 37 °C. Infections were realized at a multiplicity of infection (MOI) of 100 and incubated for 1 h at 37 °C in culture medium. After 3 washes with cellular culture medium, plates were incubated for 4, 10 and 24 h in fresh medium supplemented with gentamycin (10 μg ml^{-1}). At each kinetic point, cells were washed 3 times with culture medium and lysed by addition of 1 ml of distilled water for 10 min at 4 °C. The titer of viable bacteria was determined by spreading preparations on chocolate plates. Each experiment was conducted at least twice in triplicates.

Time Lapse Microscopy—J774–1 cells were transduced with the IncuCyte® NucLight Red Lentivirus, following the manufacturer's recommendations, to obtain red nuclear labeling of living cells because of the expression of the red fluorescent protein mKate2 containing a nuclear localization signal.

One before infection, J774–1 cells were seeded in 12-well cell tissue plates. Cells were infected (MOI of 1,000) with wild-type and mutant GFP-expressing cell. Synchronization of bacterial entry was realized by a 5 min centrifugation at 1,000 rpm. Plates were then incubated for 1 h at 37 °C in culture medium. After 3 washes with cellular culture medium, plates were incubated at 5% CO_2 and 37 °C for 24 h in fresh medium supplemented with gentamycin (10 μg ml^{-1}). Bacterial multiplication was monitored in the fully automated microscope Incucyte® S3 (Essen BioScience). Images were taken every 20 min with the 20X objective. Analysis and time-lapse videos (from which images were extracted) were generated by using Incucyte® S3 software.

Confocal Microscopy Experiments—J774.1 macrophage cells were infected (MOI of 1,000) with wild-type *F. novicida* U112, the isogenic Δ*iglB* mutant, the Δ*iglB* complemented either with wild-type *iglB* (CpWT) Y139A, Y139F mutants or an isogenic Δ*FPI* strain, in standard DMEM (DMEM-glucose) for 30 min at 37 °C. Cells were then washed three times with PBS and maintained in fresh DMEM supplemented with gentamycin (10 μg ml^{-1}) until the end of the experiment. Three kinetic points (*i.e.* 1 h, 4 h and 10 h) were sampled. For each time point, cells were washed with 1X PBS, fixed 15 min with 4% paraformaldehyde, and incubated 10 min in 50 mM NH_4Cl in 1X PBS to quench free aldehydes. Cells were then blocked and permeabilized with PBS containing 0.1% saponin and 5% goat serum for 10 min at room temperature. Cells were then incubated for 30 min with anti-*F. novicida* mouse monoclonal antibody (1/500e final dilution, Creative Diagnostics) and anti-LAMP1 rabbit polyclonal antibody (1/100e, ABCAM). After washing, cells were incubated for 30 min with Alexa488-conjugated goat anti mouse and Alexa546 conjugated donkey anti rabbit secondary antibodies (1/400e, AbCam). After washing, DAPI was added (1/1,000) for 1 min and glass coverslips were mounted in Mowiol (Citifluor Ltd.). Cells were examined using an X63 oil-immersion objective on a Zeiss Apotome 2 microscope. Co-localization tests were quantified by using Image J software; and mean

numbers were calculated on more than 500 cells for each condition. Confocal microscopy analyses were performed at the Cell Imaging Facility (Faculté de Médecine Necker Enfants-Malades).

Transmission Electron Microscopy Experiments—J774.1 macrophages were grown and infected at an MOI of 1,000 with wild-type *F. novicida* U112, or the isogenic Δ*iglB* mutantsY139A, Y139F mutants, in standard DMEM (DMEM-glucose) for 30 min at 37 °C (as described above). Twenty-four hours after infection, infected cells were fixed with glutaraldehyde 3% in phosphate buffer during one hour. Cells were then post-fixed with osmium tetroxide to stabilize lipids and enhance contrast. Sample were then dehydrated with sequential ethanol baths (from 25% to 100%) and embedded in Epon 812 resin with a 48-h polymerization time at 60 °C. Embedded samples were sliced in 90 nm thick pieces with an ultramicrotome and laid down on a copper observation grid. Image acquisitions were performed with a JEOL 1011 transmission electron microscope (tungsten filament) at the Institut Cochin (Paris, France).

BMDMs Infections—Infection of WT or *ASC*$^{-/-}$ bone marrow-derived macrophages (BMDMs) was performed as described previously (35). Briefly, BMDMs were differentiated in DMEM (Invitrogen) with 10% v/v FCS (Thermo Fisher Scientific), 15% MCSF (L929 cell supernatant), 10 mM HEPES (Invitrogen), and nonessential amino acids (Invitrogen). One day before infection, macrophages were seeded into 12- 48- or 96-well plates at a density of 2×10^5, 1.5×10^5 or 5×10^4 cells per well, respectively and incubated at 37 °C, 5% CO_2. The overnight culture of bacteria was added to the macrophages at multiplicity of infection (MOI) of 100. The plates were centrifuged for 15 min at 500 × *g* to ensure comparable adhesion of the bacteria to the cells and placed at 37 °C for 1 h. After 3 washes with PBS, fresh medium with 5 μg ml^{-1} gentamycin (Invitrogen) was added to kill extracellular bacteria and plates were incubated for the desired time.

Phagosomal Rupture Assay—Quantification of vacuolar escape using the β-lactamase/CCF4 assay (Life technologies) was performed as previously described (36). *ASC*$^{-/-}$ BMDMs seeded onto non-treated plates were infected as described above for 2 h, washed and incubated in CCF4 for 1 h at room temperature in the presence of 2.5 mM probenicid (Sigma). Propidium iodide negative cells were considered for the quantification of cells containing cytosolic *F. novicida* using excitation at 405 nm and detection at 450 nm (cleaved CCF4) or 510 nm (intact CCF4).

Sequence Analyses—To retrieve IglB homologous proteins, we used the Hidden Markov Model (HMM) profile "T6SSii_iglB.hmm" from reference (24). We scanned a dataset of 2462 predicted proteomes of complete bacterial genomes retrieved from GenBank Refseq (last accessed September 2016) using *hmmsearch* program of HMMER v.3.1b2 (gathering threshold = 25).

Our dataset included 19 genomes of the *Francisella* genus. All IglB sequences encoded by *Francisella* genomes were aligned with MUSCLE v.3.8.31 (37). Because of differences in the annotation of the first methionine codon, we used the sequence of FTN_1323 as a reference for the multiple sequence alignment.

Redundancy of the sequence set retrieved from *hmmsearch* was reduced using cd-hit-v4.6.7 (38) with a 90% identity threshold. The longest representative sequence of each cluster was then aligned with MUSCLE v.3.8.31 (37). Outliers that were very divergent in sequence length were removed. PROMALS3D and ESPript3.0 (39) servers were used to visualize multiple sequence and structure alignment using 3J9O.B PDB structure reference file (26). To determine the conservation of the phosphotyrosine site identified in *Francisella* genus (Tyr139 or Y139) we focused on the 12 amino acids surrounding the *Francisella* Tyr139 residue in the 535 aligned sequences.

To determine the conservation of the phosphotyrosine site identified in *Francisella* genus (Tyr139) we focused on the 12 amino acids surrounding the *Francisella* Y139 residue in the 535 aligned sequences. Out of the 535 aligned sequences, we found 90 sequences with a tyrosine residue in the vicinity of *Francisella* Tyr139 residue. For illustrative purpose, we selected 12 representative sequences out of 90 as shown in supplemental Fig. S3.

RESULTS

We first monitored sheath formation upon KCl stimulation, using the procedure previously described (26). Briefly, lysates of wild-type *F. novicida,* grown in the presence of 5% KC, were layered onto 15–55% sucrose gradients (Fig. 1*A*). The fraction sedimenting in equilibrium at 55% sucrose and below (55% Optiprep, gray arrow) from KCl-induced cultures were further dialyzed and used for negative staining TEM imaging. As expected, rod-shaped particles were detected by transmission electron microscopy in this fraction that corresponded to contracted sheath-like structures (Fig. 1*A* and (supplemental Fig. S2). In contrast, we failed to visualize such structures in any of the other fractions of the gradient tested.

The different fractions of the gradient were next tested by Western blotting with anti-IglA and anti-IglB antibodies. IglA and IglB were detected in all the fraction of the gradient in KCl-induced conditions (Fig. 1*B*). Because KCl induction is required to trigger sheath polymerization, we anticipated that IglA and IglB would not be detected in the lower fractions of the gradient in non KCl-induced conditions. Indeed, in the absence of KCl induction, the two proteins were only detected in the fractions of the upper half of the gradient (in the 15% and in part of the 35% sucrose fractions). We next decided to perform a whole cell proteome analysis of KCl-induced and noninduced bacterial cultures.

Whole Cell Proteome Analyses—Whole cell extracts from KCl-induced and noninduced cultures were analyzed to identify proteins whose abundance was altered by the KCl treatment. We could quantify 1,395 proteins that represent 80% of the predicted *Francisella* proteome (supplemental Table S3). Upon KCl stimulation, 113 proteins were up-regulated after KCl stimulation and 97 down-regulated, confirming that KCl stimulation strongly alters the proteome of the cell (supplemental Table S3, Fig. 1*C*). Remarkably, the amounts of most of the FPI-encoded proteins (17 out the 18 proteins encoded by the FPI were identified) did not change significantly upon KCl stimulation, including notably the sheath and tube proteins IglA, IglB, IglC (blue dots in Fig. 1*C*).

The down-regulated proteins included seven proteins (FTN_0042 to FTN_0048) encoded by the "*Francisella novicida* island" (or FNI), a genomic island that shows some similarities with the FPI (35), where FTN_0042 and FTN_0043 correspond to the orthologues of IglA and IglB, respectively). Oppositely, two sets of proteins emerged as up-regulated (supplemental Fig. S3*A*): proteins involved in Iron-sulfur (Fe/S) clusters biogenesis (FTN_0751 to FTN_0754, FTN_0850 to FTN_0853 and FTN1082) as well as most of the protein encoded by the *fig* (also designated *fsl*) operon (41, 42), involved in iron acquisition (FTN_1681, FTN_1682, FTN_1684 to

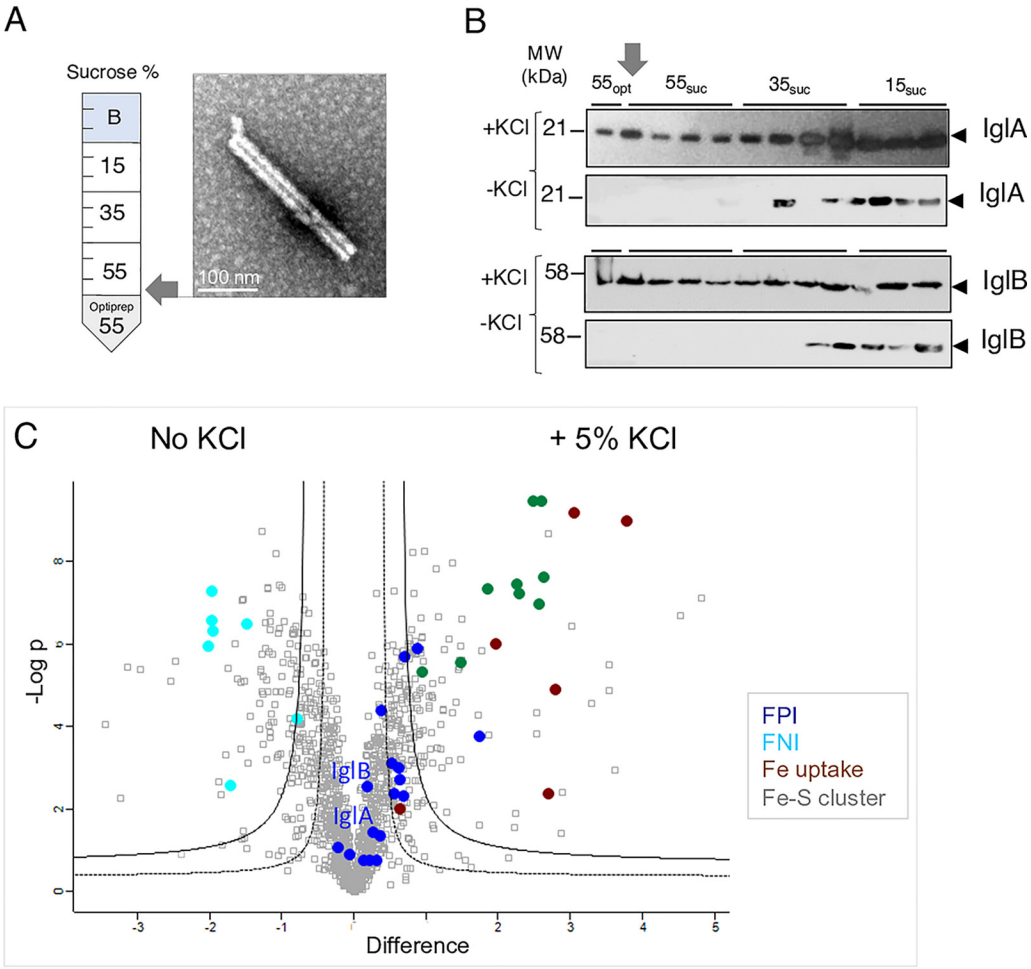

FIG. 1. **KCl stimulation of sheath formation.** *A*, Sucrose gradient. Lysates of bacteria grown in Schaedler K3 medium in the presence of KCl were laid on top of a discontinuous sucrose gradient 15–55%/Optiprep 55%. Left panel, composition of the gradient; Right panel, transmission electron microscopy (TEM) of the "heavy" fraction (gray arrow, topping the Optiprep cushion). The assembled sheath-like structure, sedimenting at equilibrium to below 55% sucrose, are rod-shaped particles of variable length (100 - 600 nm). One prototypical sheath-like structure is shown. *B*, Western blot analysis of the different fractions, using anti-Igl (A, B or C) antibodies. The gray arrow corresponds to the fraction topping the Optiprep cushion. *C*, The proteome of KCl-stimulated and nonstimulated *F. novicida.* Volcano plot representing the statistical comparison of the protein LFQ intensities of KCl- stimulation *versus* nonstimulated cells. Inner volcano was established using S0 = 0.5, FDR = 0.01 (class B proteins) and the outer volcano using S0 = 0.5, FDR = 0.001 (class A proteins). Proteins belonging to the FPI, the Fe uptake and Fe-S clusters are highlighted in color as indicated.

FTN_1687) (supplemental Fig. S3*B*). On the basis of the known regulation of Fe/S clusters in other bacterial species (43, 44), these Fe/S cluster proteins could be regulated by FTN_0810, a predicted transcriptional regulator sharing modest sequence identity with the Fe/S regulator IscR.

The fact that the amounts of T6SS proteins remained unchanged upon KCl induction, led up to hypothesize that a post-translational mechanism might be responsible for KCl-dependent sheath polymerization.

The Phosphoproteome of Francisella—Our careful inspection of the *Francisella* genomes did not identify any gene encoding for a putative serine/threonine-protein kinase or tyrosine kinase. Despite this lack of canonical kinases, we hypothesized that serine/threonine/tyrosine phosphorylation of proteins might occur in *Francisella* and contribute to pathogenesis. We therefore carried out a global and site-specific phosphoproteomic analysis of *F. novicida* (strain U112), based on phosphopeptide enrichment and high-resolution LC-MS/MS analysis from KCl-induced and noninduced cultures (Fig. 2). Overall, this analysis allowed the identification of 103 phosphopeptides, of which 78 were robustly quantified. The majority of the phosphosites (47 out of 78) were found on serine residues (S), whereas similar lower number of sites, 19 and 12, were found on threonine (T) and tyrosine (Y), respectively (Fig. 2*A*, 2*B*; supplemental Table S4). These phosphosites corresponded to 59 proteins, of which 7 presented multiple phosphorylation sites. These proteins belonged to various functional categories and the most represented classes were carbohydrate metabolism, energy production and conversion and translation.

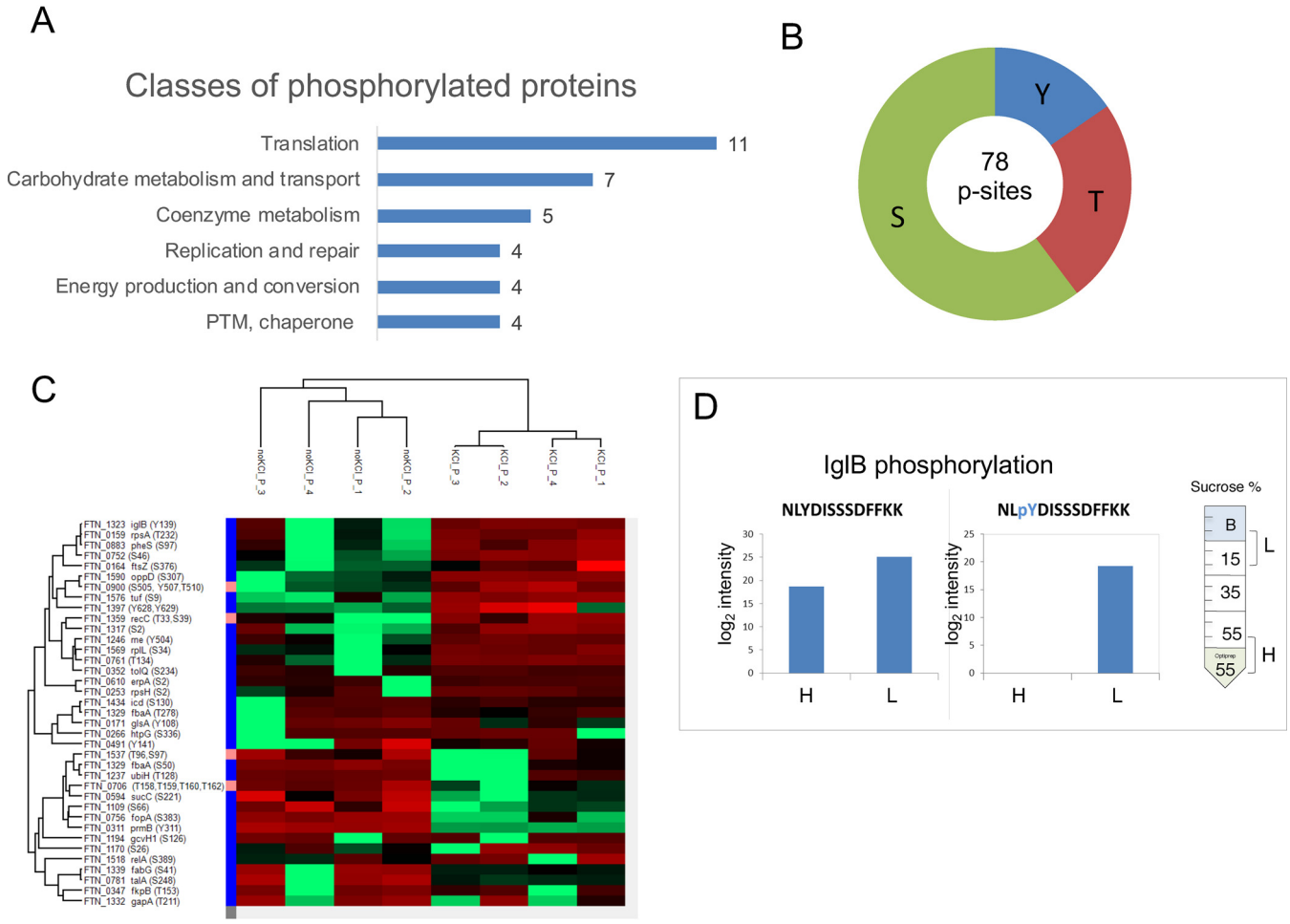

FIG. 2. **The phosphoproteome of *F. novicida*.** *A*, Histograms of the most represented classes of protein. The values correspond to the number of proteins bearing phosphosites in each category. *B*, Distribution of phosphosites according to the modified amino acid (tyrosine,Y; threonine,T and serine, S). *C*, Heat map of phosphoproteins altered upon KCl stimulation (Pink to right of the FTN numbers corresponds to proteins with multiple phosphorylation sites). The black arrow is pointing to Y139 of IglB. D, IglB phosphorylation distribution. Intensities (in log2) of the nonphosphorylated (left) and phosphorylated (right) Tyr139-containing peptide in the "heavy" (H) and "light" (L) fractions, respectively. The signal of the phosphopeptide was only detectable after phosphoenrichment. nd, not detectable.

The phosphopeptide NLY(Phospho)DISSSDFFK fragmentation spectrum is available on MS-Viewer (key lkaqkllxwx, scan number 38578).

IglB was the only protein of the T6SS that we found to be phosphorylated on Y139, particularly after KCl stimulation (Fig. 2*C*). As mentioned above, IglB constitutes with IglA the T6SS sheath of *Francisella* (17, 26, 35).

Y139 Is a Conserved Amino Acid—Comparative sequence analyses on 33 IglB proteins from 19 genomes of the *Francisella* genus were performed to assess the conservation of residue Tyr139 (supplemental Fig. S4). Sequences were highly conserved between 31 IglB proteins sharing 93 to 100% amino acid identity. In contrast, the proteins encoded by *FTN_0043* in the FNI (35) and *F7308_1917* (Fsp_TX077308) exhibited only 48% amino acid identity with the 31 other IglB proteins whereas they both share 85% identity. Excluding these 2 outliers, among 506 sites, 458 were without polymorphism (91%), with Tyr139 conserved in all IglB sequences (supplemental Fig. S4, upper part). Because IglB is among the most conserved components of T6SS (17, 26), we were able to retrieve orthologues of IglB encoded outside of *Francisella* genus. Out of 535 nonredundant IglB orthologues (also named VipB, TssC or EvpB/VC_A0108), we found 90 sequences with a tyrosine in the vicinity of Tyr139 site outside of *Francisella* genus. In 82 sequences, the predicted location of the tyrosine residue was like that of Tyr139 (in a turn region between two helices) (supplemental Fig. S4, lower part).

IglB phosphorylation in sheath formation—To determine if the phosphorylated forms of IglB was incorporated into the sheath upon its assembly, we further compared the phosphoprotein content of the fractions at the bottom of the gradient (sucrose 55%-Optiprep 55% density zone), containing the sheath-like particles, to the fractions at the top of the gradient (15–35% sucrose density zone), presumably containing non-polymerized forms of the IglA and IglB proteins (hereafter called "heavy fraction," H or "light fraction," L, respectively) (Fig. 2*D*, supplemental Table S5).

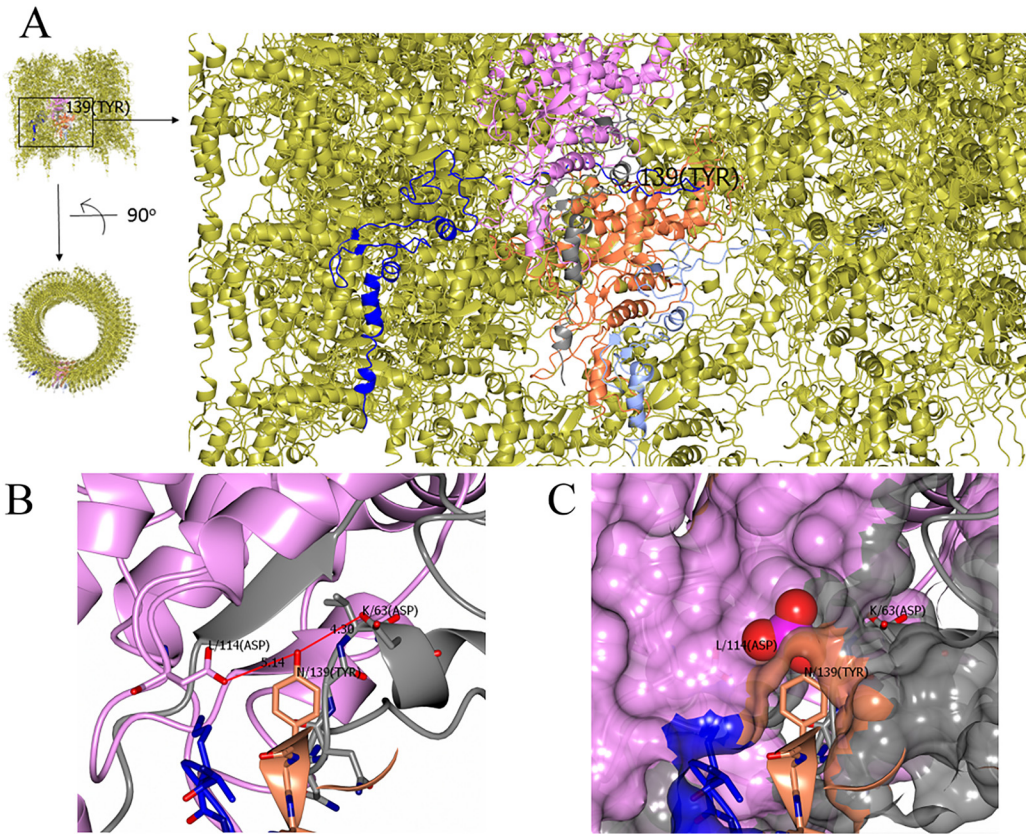

FIG. 3. **Predicted role of Y139 of IglB in sheath assembly.** *A*, Overview of the sheath that consists of 12 helical strands based on EM reconstruction at 3. 7 Å (PDB 3j9o PDBe biological assembly1). The strands are built of IglA/IglB dimers. IglBTyr139 of the coral IglB/light blue IglA dimer lies close to the gray/pink IglA/B dimer in the same strand. It also lies close to the N-terminal extension of the dark blue IglA from an adjacent strand. The chain coloring is used in the rest of the panels of this figure. *B*, Close up of the region of Tyr139. The hydroxyl is pointing into a pocket and not obviously making a Hydrogen bond. However, the carboxylates of Asp114 from IglB and Asp63 of IglA in the next dimer are around 5 Å away. At the resolution of the reconstruction side chain density is not well defined and these could in fact be close enough to H bond. *C*, Surface of the assembly clipped to show Tyr139. There is enough space for a phosphogroup on the Tyr. The two Asps will however be close to the phosphogroup and so there is likely to be charge repulsion impairing the sheath assembly, or weakening the sheath stability, when Y139 is phosphorylated.

The mass spectrometry analysis of the H and L fractions identified over 1145 proteins (supplemental Table S6) and confirmed the efficiency of the sucrose gradient separation. Unmodified peptides containing Tyr139 were detected in both H and L fractions, indicating that soluble IglB include both phosphorylated and nonphosphorylated forms of the protein. Importantly, the peptide bearing the phosphorylated tyrosine residue (pY139) of IglB was only detected in the L fraction of the gradient (supplemental Table S5), suggesting that tyrosine phosphorylation might be unfavorable for sheath polymerization.

Fully supporting this notion, our 3D predictions (Fig. 3) indicate that, upon addition of a phosphoryl moiety at this position, charge repulsion between the phosphate group and nearby aspartate residues should be unfavorable for the formation of stable hexameric rings and sheath contraction. Because the phosphate on Y139 is linked to the O^4 position of the phenolic ring, the effects of Tyr phosphorylation may be exerted primarily through allosteric/electrostatic effects. Looking at the full helical reconstruction, one can see that Y139 is close to both D63 of IglA and D114 of IglB. These are from two different symmetry-related chains (Fig. 3). Putting a phosphate on Y139 is thus likely to repel the aspartate residues and to disassemble the structure.

Functional Assays to Understand the Role of Phosphorylation on Y139—We hereafter thoroughly evaluated the importance of Y139 phosphorylation on T6SS functionality and *Francisella* pathogenicity. For this, we constructed two IglB variants in which Tyr139 was substituted either by an alanine (A) or by the nonphosphorylatable aromatic amino acid analogue of tyrosine, phenylalanine (F). These IglB mutated proteins (designated Y139A and Y139F, respectively) were expressed *in trans* in a Δ*iglB* mutant of *F. novicida* carrying a chromosomal deletion of the entire *iglB* gene, (see Materials and Methods). A mutant with a deletion of the entire *FPI* (Δ*FPI*) and a Δ*iglB* deletion mutant were used as negative controls. Both mutants are unable to escape from phagosomes and hence to grow in macrophages (45).

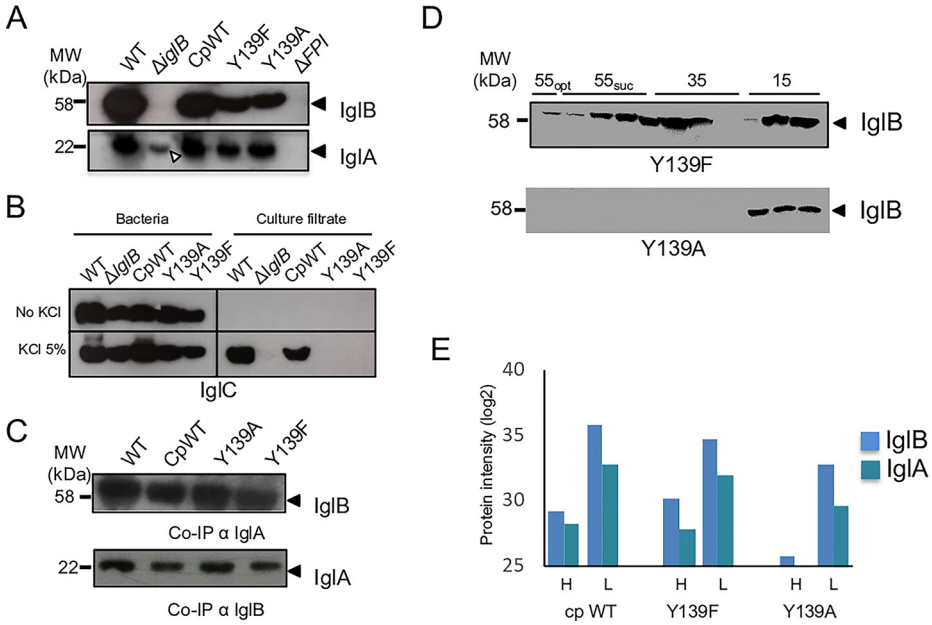

FIG. 4. **Immunodetection of IglA, IglB and IglC in wild-type and IglB mutant strains.** *A*, Western Blots (WB) of whole cell protein extracts. Upper gel: WB with anti-IglB; lower gel: WB with anti-IglA. *B*, Western Blots (WB) with anti-IglC on bacteria/culture filtrates. Bacteria were grown in Schaedler-K3 supplemented or not with 5% KCl until late log phase and then harvested by centrifugation. Culture supernatants were collected after filtration on 0.2 μM Millipore filters and concentrated using Amicon 3 kDa membranes. The equivalent of 200 μg of total protein were loaded onto each well. Upper gel, bacterial cultures grown without KCl; lower gel, bacterial cultures supplemented with 5% KCl. *C*, Co-immunoprecipitations (Co-IP). Upper gel: IP-anti-IglA, followed by WB with anti-IglB; lower gel: IP-anti-IglB, followed by WB with anti-IglA. *D*, WBs of sucrose gradient fractions of the Y139F and Y139A mutant strains. *E*, Distribution of the intensities (trasformed in log 2) of the proteins IglA and IglB in the Heavy (H) and light (L) sucrose fraction, in cp WT (Δ*iglB* complemented with WT IglB), Y139F and Y139A (Δ*iglB* complemented with IglB Y139F and IglB Y139A, respectively).

IglB was detected by Western blotting on whole cell lysates in wild-type and complemented mutated strains (Y139A and Y139F) but not in the Δ*iglB* and Δ*FPI* strains (Fig. 4*A*). IglA was also detected in wild-type and complemented mutated strains (Y139A and Y139F), but in lower amounts in the Δ*iglB* strain and not in the Δ*FPI* mutant. This observation agrees with earlier observations (46) that suggested that the presence of IglB increases the stability of IglA.

A classical measure of basal T6SS function is the export of an Hcp-related protein (IglC in *F. novocida*). Therefore, we examined IglB-dependent IglC export in the different *F. novicida* mutant strains by Western-blot on bacteria grown in the presence -or absence- of 5% KCl. In agreement with previous reports, IglC was detected in the culture supernatant in the presence, but not in the absence, of KCl, in the wild-type and $iglB_{WT}$ complemented strains. In contrast, deletion of *iglB* as well as the two single amino acid substitutions Y139A and Y139F, all abolished the secretion of IglC into the culture medium (Fig. 4*B*, right). We also verified that it is because of secretion impairment as KCl treatment did not modify the amounts of IglA, IglB and IglC proteins detected by Western blotting on whole cells (bacterial pellet fractions) (Fig 4*B*, left). These results confirmed the proteomics data (Fig 1*C*).

To check the impact of the two amino acid substitutions on IglA-IglB heterodimer formation, we performed co-immunoprecipitation assays (Fig. 4*C*). We used either anti-IglA to precipitate the complex, followed by Western blotting with anti-IglB (upper panel) or anti-IglB, followed by Western blotting with anti-IglA (lower panel). In both conditions, the two IglB mutants were still able to interact with IglA to form IglA-IglB heterodimers.

We next performed sucrose gradient fractionation (as described above), followed by Western blotting with anti-IglB on the Y139F and Y139A mutant strains. The Y139F IglB mutant protein was detected in both the L and H fractions of the gradient (Fig. 4*D*), indicating that some sheath polymerization still occurred in the Y139F mutant. In contrast, the Y139A mutant protein was detected in the upper fractions of the gradient but not in the lower fractions (corresponding to the contracted sheath). Fully supporting the western-blot data, proteomic analysis of the distribution of IglA and IglB in the Heavy (H) and light (L) sucrose fraction revealed that their distribution was similar in the strains expressing either WT IglB and Y139F IglB with, in both case, a slightly higher proportion of IglA and IglB in the L fraction compared with the H fraction. In sharp contrast, with the Y139A mutant, IglB was absent from the H fraction and IglA also almost exclusively found in the L fraction (Fig. 4*E*; supplemental Table S6).

Critical Role of Residue Y139 in Francisella Pathogenesis—The mutations Y139A and Y139F had no effect on bacterial growth in broth (supplemental Fig. S5). We therefore decided

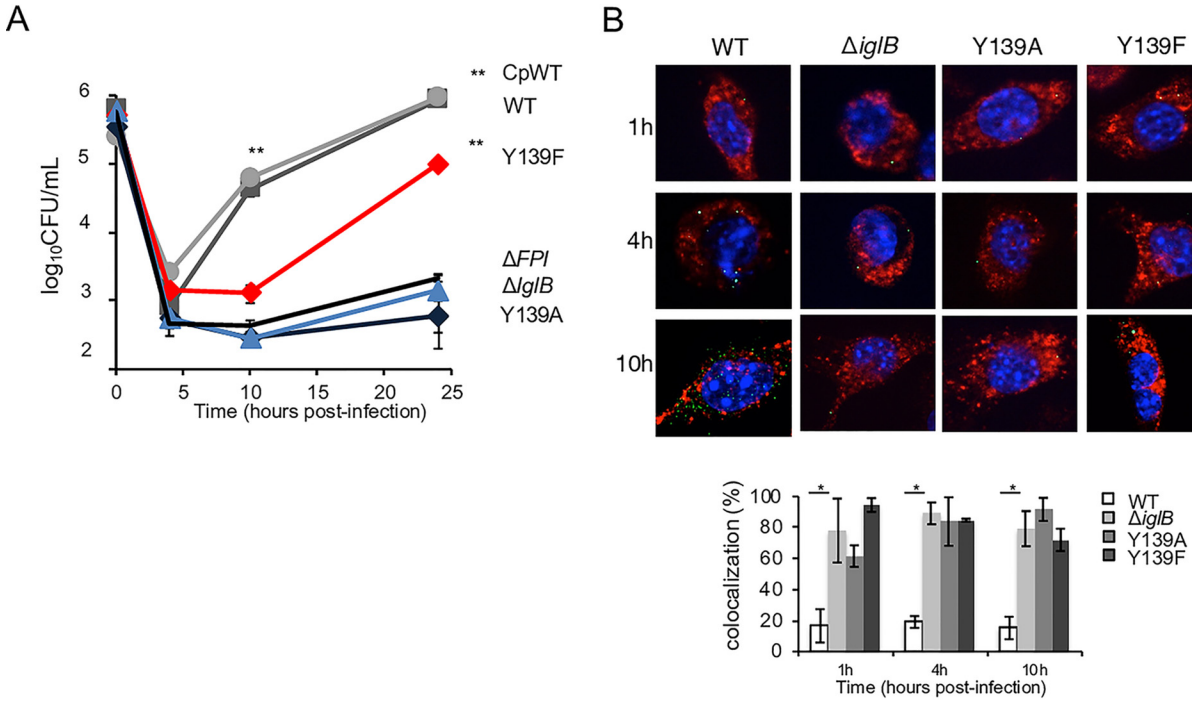

FIG. 5. **Y139Aand Y139F IglB mutants show impaired intracellular survival in J774–1 macrophages.** *A*, Intracellular bacterial multiplication of wild-type *F. novicida* (WT, Gray squares), isogenic Δ*iglB* mutant (Δ*iglB*, blue triangles) and complemented Δ*iglB* strain (Cp-WT, gray circles; Y139A, blue square; Y139F, red squares) and the Δ*FPI* control (black lines), was monitored during 24 h in J774A.1 macrophage cells. The values recorded for Y139F, at 24 h, were significantly different from those of Δ*FPI*, Δ*iglB* or Y139A. In both cell types, the values recorded for WT or CpWT, at 10 h and 24 h, were significantly different from those of Δ*FPI*, Δ*iglB,* Y139A or Y139F. $^{**}p < 0.001$ (determined by student's *t* test). *B*, Confocal microscopy of intracellular bacteria with J774–1 infected with wild-type *F. novicida* (WT), Δ*iglB* or complemented strains and their co-localization with the phagosomal marker LAMP1 observed at 1 h, 4 h and 10 h. Upper par: J774.1 were stained for *F. novicida* (green), LAMP-1 (red) and host DNA (blue, DAPI stained). Lower part: analysis was performed with ImageJ software. $^{*}p < 0.01$ (determined by student's *t* test).

to verify the ability of wild-type *F. novicida* (WT), Δ*iglB* and complemented strains (CpWT, Y139A and Y139F) to survive and multiply in murine macrophage-like J774.1 cells over a 24 h-period (Fig. 5*A*). Confirming earlier reports (47), intracellular multiplication of the Δ*iglB* mutant was essentially abolished and comparable to that of the Δ*FPI* mutant. The single amino acid substitution of Y139 by an alanine (Y139A) also abolished intracellular bacterial multiplication. In contrast, when Y139 was substituted by a phenylalanine (Y139F), although cytosolic growth was prevented until 10 h after infection, at 24 h the Y139F mutant strain had actively multiplied (ultimately leading to only a 10-fold reduction of bacterial counts compared with wild-type). As expected, functional complementation (*i.e.* introduction of a plasmid-born wild-type *iglB* allele into the Δ*iglB* mutant strain (CpWT) restored wild-type growth.

To confirm that a late phagosomal escape had occurred in the Y139F mutant, we next compared the ability of the Δ*iglB* mutants to escape from the phagosomal compartment to that of the wild-type strain, by monitoring co-localization of intracellular bacteria with the phagosomal marker LAMP-1, (Fig. 5*B*) up to 10h after infection in J774–1 macrophages. Co-localization of the wild-type strain with LAMP-1 was below 20% as soon as 1 h after infection. In contrast, the frequency of bacteria co-localizing with LAMP-1 remained elevated (between 60 and 90%), with Δ*iglB (*as expected), but aso with Y139A and Y139F. In agreement with the kinetics data, this assay confirmed that whereas the wild-type strain had already escaped into the host cell cytosol at 1 h, the Y139A and Y139F mutants were still trapped in the phagosomal compartment at 10 h.

Transmission electron microscopy confirmed that a clear cytosolic multiplication was visible at 24 h with the Y139F mutant but not with the Y139A mutant (Fig. 6*A*), fully supporting the kinetics and confocal data (Fig 5*A*). We therefore next used time-lapse video microscopy to visualize in real time multiplication of the Y139F mutant in J774–1 macrophages. For this, we inserted a GFP-encoding gene into plasmids pKK214::pGro*iglB* and pKK214::pGro*iglB*Y139F (yielding recombinant plasmids pKK214::pGro*iglB*-pGro*gfp* and pKK214::pGro*iglB*Y139F- pGro*gfp,* respectively). *F. novicida* Δ*iglB* was transformed with these GFP-expressing recombinant plasmids. We generated J774–1 cells with red nuclei by transduction with NucLight Red Lentivirus to facilitate cell recognition and counting (see Materials and Methods). J774–1 cells with red nuclei were infected by GFP-expressing bacteria at an MOI of 1000. Infection was followed over a 24 h-period, using a fully auto-

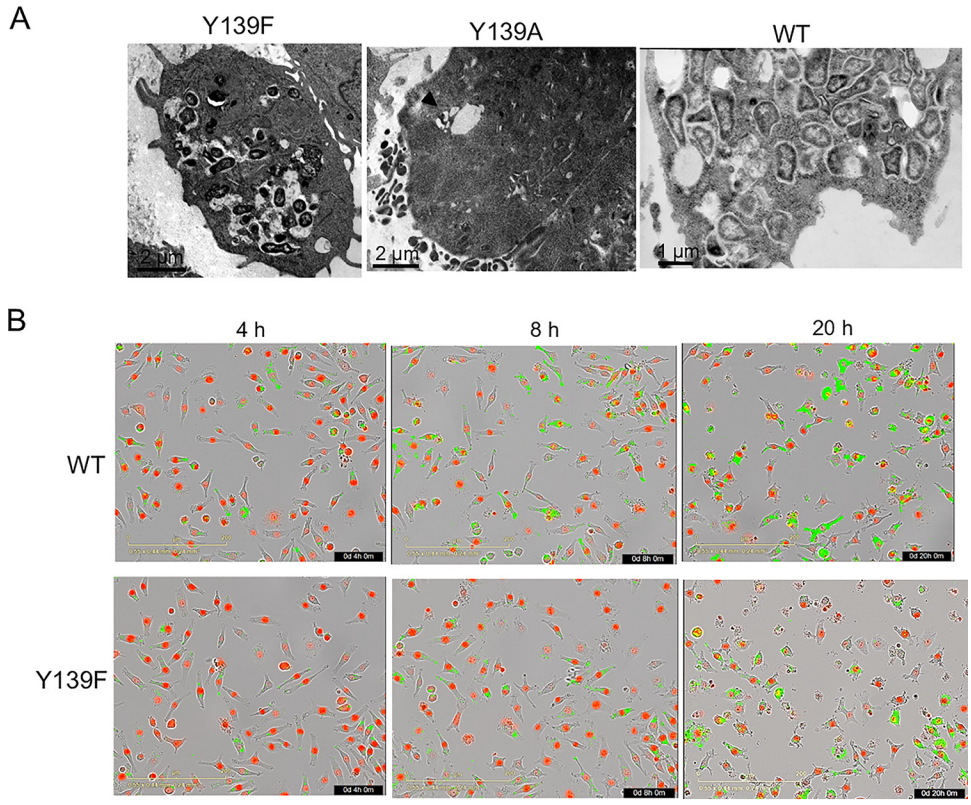

FIG. 6. **Electron microscopy and time lapse video microscopy.** *A*, Transmission electron microscopy of J774–1 cells infected with Y139F, Y139A or WT *F. novicida* at 24 h. Active bacterial multiplication was visible in the cytosol of both WT- and Y139F-infected cells (first and third panels show a single cell infected with multiple bacteria). In contrast, only rare bacteria could be visualized withY139A-infected cells. The middle panel shows one cell infected with a unique bacterium (the black arrowhead points to a single bacterium still entrapped in a vacuolar compartment). *B*, Time lapse video microscopy. J774–1 cells expressing a nuclear restricted Red Fluorescent Protein were infected with GFP-expressing WT and Y139 IglB proteins. Representative images were taken at 4 h, 8 h and 20 h (see supplemental Video S1 and S2). Red: cell nuclei. Green: GFP expressing bacteria.

mated microscope Incucyte® 531 S3 (Essen BioScience). Images were taken every 20 min with the 20X objective during 24 h, starting 1 h after infection (Fig. 6*B*; supplemental Videos S1, S2).

Hence, in perfect agreement with the kinetics and electron microscopy data, time-lapse video microscopy confirmed that, despite an initial delay in bacterial multiplication because of altered phogosomal escape (up to10 h of infection), the Y139F mutant was capable of active cytosolic multiplication at later time points. Hence, it is likely that the Y139F substitution allows the production of enough assembled T6SS to promote bacterial phagosomal escape and cytosolic multiplication in these cells.

We also replaced Tyr139 by two phosphomimetics *i.e.* the negatively charged amino acids Aspartate and Glutamate and evaluated the impact of these amino acid substitutions (Y139D and Y139E) on intracellular multiplication in J774–1 cells (supplemental Fig. S6*A*). The two mutants led to severe defects in intracellular multiplication and, at all time points tested, the replication defect was comparable to that of the Y139A or Δ*FPI* mutant. We next evaluated the capacity of the Y139D and Y139E mutants to form sheath-like structure by using the sucrose gradient assay. In the two mutants, the IglB protein was exclusively detected by Western blotting in the upper fractions of the sucrose gradient (supplemental Fig. S6*B*). These data strongly suggest that residues possibly mimicking the phosphorylated state of Y139 also prevented sheath-like assembly.

Functional Assays in Primary Cultures—Finally, we evaluated the ability of Y139A and Y139F mutants to multiply in primary bone marrow-derived macrophages (BMMs) over a 24 h-period. In these cells, growth of both Y139A and Y139F mutants was like that of Δ*FPI* and Δ*iglB* mutant strains (supplemental Fig. S7*A*) even at 24 h. The ability of the Y139A and Y139F mutants to induce phagosomal membrane rupture in BMMs was also tested using the β-lactamase/CCF4 assay (35, 48). Strains expressing wild-type IglB showed similar amount of cleaved CCF4 at all time-points tested whereas there was no (or marginal) loss of FRET signal with Δ*iglB*, Y139A, Y139F, and the two negative control strains, confirming that the Y139A, Y139F mutant strains remained stuck in intact phagosomes during at least the first 6h hours of infection also in these cells (supplemental Fig. S7*B*).

DISCUSSION

This is the first report of protein phosphorylation events in *Francisella.* Our proteomic approaches allowed the identification of a unique residue of the T6SS sheath that is phosphorylated and that plays a critical in phagosomal escape of this pathogenic bacterium.

Pivotal Role of Tyrosine 139 of IglB in Sheath Assembly—Formation of the *Francisella* T6SS is believed to occur in the phagosome before the escape of the bacterium in the cytosol. Once in the cystosol, the T6SS seems to be dispensable for cytosolic multiplication. Nevertheless, some T6SS elements are likely to be required during the cytosolic stage of the infectious cycle. Indeed, most FPI genes are induced during late intra-macrophage growth (49) and IglC has been shown to be required for intracellular growth of *F. novicida* that are microinjected directly into the cytosol of HeLa cells (21). IglC secretion in *F. novicida* depends on the T6SS core components IglA and IglB (50). Of note, truncated IglA proteins still able to form IglA/IglB-heterodimers have been reported to have lost their IglC secretory function (26), suggesting that heterodimer formation is not enough to generate a functional sheath.

We showed that the single substitution of IglB residue 139 either by alanine, aspartate or glutamate (Y139A, Y139D or Y139E) was enough to abrogate T6SS assembly, prevent phagosomal escape and abolish intracellular bacterial multiplication. Of note, these three amino acid substitutions eliminate the phenol ring. In contrast, the substitution Y139F, which preserves the phenol ring but not the phosphorylatable OH moiety, could still assemble possibly unstable sheath-like structure (Fig. 4*D*, 4*E*) and allow bacterial multiplication in J774–1 macrophages (Fig. 5*A*; Fig. 6*A*, 6*B*; supplemental Video S2). Indeed, the kinetics of intracellular multiplication, the electron microscopy and time-lapse video microscopy assays all confirmed that, despite an altered phagosomal escape, the Y139F mutant was able to access the cytosolic compartment and promote active multiplication in this compartment.

Of note, we found that multiplication of the Y139F was abrogated in primary bone marrow-derived macrophages, probably because of the high bactericidal activity of these cells. Altogether these data support the notions that: (1) both the phenol ring steric hindrance and the OH moiety are key to T6SS assembly; and (2) the phosphorylation of OH on the Y139 is not favorable to sheath polymerization. At this stage, the inability of the Y139F mutant to form stable T6SS might be explained by the fact that it maintains the phenol rings but it lacks the OH moiety. Of note, it was demonstrated that a single tyrosine Hydroxyl Group controlled the specificity of *Plasmodium falciparum* ferredoxin-NADP+ reductase (51).

Although inspection of the 3.7 Å EM reconstruction of the *F. novicida* contracted sheath (PDB 3j9o) does not show any atoms close enough to form a hydrogen bond with the hydroxyl of Y139, the carboxylates of D114 from IglB, and D63 of IglA in the next dimer, are around 5 Å away and these may approach close enough to Y139 OH to form hydrogen bond interactions stabilizing the assembly. 3D modeling also indicated that there is space for a phosphate group on this atom as the OH is pointing into a pocket in the structure (Fig. 3). However, the negatively charged phosphate would induce charge repulsion with the nearby Asps from the next dimer most likely preventing assembly of the strands when Y139 is phosphorylated. Hence, the charge repulsion provoked by addition of the phosphorylation moiety (when Y139 is phosphorylated) is likely to weaken the stability of the contracted sheath. Altogether these data suggest that the phosphorylation status of IglB could modulate T6SS assembly/disassembly process. Supporting the notion that phosphorylation of Y139 impairs sheath contraction, replacement of this residue by a phosphomimetic (Y139D or Y139E) led to a severe intracellular multiplication defect and prevented sheath-like structure formation.

IglB Phosphorylation, a New Mediator of T6SS Dissociation?—The assembly of the T6SS-H1 of *Pseudomonas aeruginosa* has been shown to be spatially regulated by a post-translational mechanism coined "The Threonine Protein Phosphorylation" (or TPP) Pathway. During this process, involved in the defense of bacteria to a neighboring attack, a membrane-bound threonine kinase phosphorylates a forkhead-associated domain-containing Protein (FhA or TagH), which promotes the assembly of an active conformation of the T6SS at the site of the attack (52–54). Recently, the offensive anti-bacterial T6SS of *Serratia marcescens* has also been shown be controlled by the opposing actions of the TPP pathway and TagF on assembly of the core machinery (55). The TPP represents the only currently identified post-translational mechanism regulating T6SS biogenesis. Because the *Francisella* genomes do not encode any putative tyrosine kinase, yet unidentified protein(s) with a noncanonical tyrosine kinase activity may be responsible for IglB phosphorylation.

In contrast to all the canonical T6SS, the FPI does not encode any homologue of the unfoldase ClpV, but instead uses the general chaperone ClpB for the recycling of the contracted sheaths. Indeed, Basler and co-workers have recently shown that *F. novicida* assembled its T6SS sheath on the bacterial poles and that the sheath cycled through assembly, contraction and disassembly, similarly to what was previously described for other canonical T6SSs (7). ClpB was shown to specifically localize with the contracted sheaths and is responsible for their disassembly within phagosomes of infected macrophages. Interestingly, the amounts of ClpB were not (or marginally) up-regulated upon KCl induction (*i.e.* only 1.3-fold more ClpB in KCl-induced conditions compared with noninduced conditions). ClpB was also mainly associated with the soluble fraction of the sucrose gradient of KCl-induced bacteria). IglB phosphorylation might assist ClpB when the sheath is contracted to promote its dissociation (Fig.

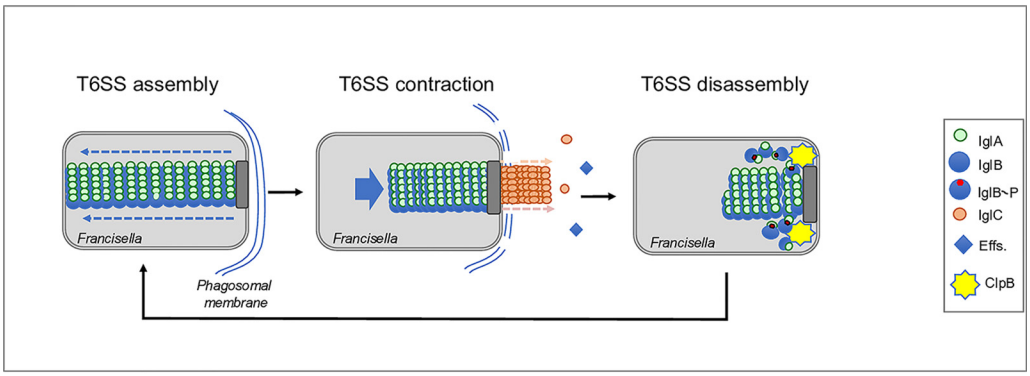

FIG. 7. **Model of T6SS dynamics.** Schematic depiction of the three major steps of the T6SS dynamics. Proposed contribution of IglB phosphorylation to T6SS disassembly.

7). The kinase activity leading to IglB phosphorylation might assemble, like ClpB, at the pole of the bacterium only when the sheath is contracted and assist sheath dissociation. However, our careful inspection of the *Francisella* genomes did not identify any gene encoding for a putative serine/threonine- or tyrosine-kinase.

Of note, two proteins, FTN_0459, predicted to encode a UbiB kinase, and the histidine kinase kdpD, were found to be phosphorylated (on T128, T165/S166, S176 and T173 for UbiB and on S670 for KdpD; supplemental Table S4). The UbiB protein family is a widespread family of kinase-like present in the three kingdoms of life, often required for the biosynthesis of isoprenoid lipids. In Escherichia coli, UbiB has been shown to be required for the aerobic biosynthesis of the redox-active lipid ubiquinone, coenzyme Q (56). It has been assumed but not formally established that UbiB family members were protein kinases. Two-component systems (TCS) are known to be involved in multiple physiological responses and the regulation of virulence in many bacteria. These signal transduction systems involve two proteins: a sensing protein and a transcription factor. The membrane sensor is a histidine kinase that mediates phosphotransfer to a DNA-binding regulatory protein with a phosphorylated aspartate phosphoacceptor site that alter the level of gene expression. *F. novicida* has two complete TCS, including KdpD (the histidine kinase FTN_1715)/KdpE (the regulatory protein FTN_1714) (57). KdpD, whose predicted phosphorylation site is Histidine 674, has been also shown to be responsible for the phosphorylation of protein FTN_1465 (also designated QseB or PmrA) at the aspartic acid at position 51, suggesting the existence of possible crosstalks between complete and incomplete TCS in Francisella. However, possible correlations between such kinases and tyrosine phosphorylation remain purely speculative.

This suggests that a yet unidentified enzyme with either a noncanonical tyrosine kinase activity or a protein predicted to be involved in a different enzymatic reaction with a ≪ moonlight ≫ tyrosine kinase activity, is responsible for IglB phosphorylation. If so, its identification might prove extremely difficult and would require extensive future work. It is also possible that a single kinase mutant might have no or very limited effect on phagosomal disruption because sheath polymerization would occur and be enough to promote phagosomal membrane disruption. Indeed, it has been shown (21) that only a minor fraction of functional T6SS is enough to promote phagosomal escape and, once in the cytosol, FPI mutants can multiply like wild-type bacteria.

In bacteria such as *Escherichia coli, Vibrio cholerae* or *Pseudomonas aeruginosa*, the sheath contracts spontaneously during the repeated rounds of ultraspeed purification required for their isolation from cell cultures (58). In *Francisella*, T6SS contraction can be triggered in culture either by placement under coverslips or by KCl stimultation (26). We found in this study that the amounts of more than two hundred proteins were altered upon KCl stimulation (Fig. 1). Hence, proteins that were up-regulated upon KCL stimulation might also contribute to T6SS biogenesis (such as proteins involved in Iron-sulfur clusters biogenesis or in iron acquisition). Notably, the down-regulated proteins comprized seven proteins (FTN_0042 - FTN_0048) out of the 13 proteins potentially encoded by the *Francisella novicida* island (FNI, FTN_0042 - FTN_0054) (35). Although inactivation of the whole FNI locus had no effect on *F. novivcida* virulence, a possible contribution of the orthologues of IglA and IglB (FTN_0042 and FTN_0043) to the sheath assembly-disassembly process cannot be excluded.

In conclusion, our mass spectrometry analyses revealed that the sheath protein IglB was the only T6SS component to contain a phosphorylatable residue (Y139). Importantly, our functional assays demonstrated that Y139 played a critical role in functional T6SS assembly.

Acknowledgments—We thank Dr A. Sjostedt for providing the *F. novicida* strain U112 and Alain Schmitt (Cochin Institute Electron Microscopy Facility) for excellent technical support.

DATA AVAILABILITY

The mass spectrometry proteomics data have been deposited to the ProteomeXchange Consortium via the PRIDE (40) partner repository with the dataset identifier

PXD013619. Annotated spectra can be viewed on MS-Viewer (http://msviewer.ucsf.edu/prospector/cgi-bin/msform.cgi?form=msviewer) with the search key lkaqkllxwx.

* These studies were supported by INSERM, CNRS and Université Paris Descartes Paris Cité Sorbonne. Jason Ziveri was funded by a fellowship from the "Délégation Générale à l'Armement". Claire Lays was funded by a fellowship from the LABEX ECOFECT (ANR-11-LABX-0048) of Université de Lyon, within the program "Investissement d'Avenir" (ANR-11-IDEX-0007) operated by the French National Research Agency (ANR). No author has an actual or perceived conflict of interest with the contents of this article.

[S] This article contains supplemental material.

** To whom correspondence may be addressed. Tel.: 33 172 60 65 11; Fax: 33 1 - 72 60 65 13; E-mail: alain.charbit@inserm.fr.

‡‡ To whom correspondence may be addressed. Tel.: 33 172 60 65 11; Fax: 33 1 - 72 60 65 13; E-mail: chiara.guerrera@inserm.fr.

§§ Present address: 156–160 Rue de Vaugirard, 75015 Paris, France.

Author contributions: J.Z., M.B., M.C., T.H., I.C.G., and A.C. designed research; J.Z., C.C., H.R., G.P., F.T., and C.L. performed research; J.Z., A.J., M.C., C.L., N.H.K., I.C.G., and A.C. analyzed data; C.C. and T.H. contributed new reagents/analytic tools; N.H.K., I.C.G., and A.C. wrote the paper.

REFERENCES

1. Sjostedt, A. (2007) Tularemia: history, epidemiology, pathogen physiology, and clinical manifestations. *Ann. N.Y. Acad. Sci.* **1105,** 1–29
2. Sjostedt, A., ed. (2011) *Francisella tularensis and tularemia*, Fontiers Media SA
3. Luque-Larena, J. J., Mougeot, F., Arroyo, B., Vidal, M. D., Rodriguez-Pastor, R., Escudero, R., Anda, P., and Lambin, X. (2017) Irruptive mammal host populations shape tularemia epidemiology. *PLoS Pathog.* **13,** e1006622
4. Maurin, M., and Gyuranecz, M. (2016) Tularaemia: clinical aspects in Europe. *Lancet Infect. Dis.* **16,** 113–124
5. McLendon, M. K., Apicella, M. A., and Allen, L. A. (2006) Francisella tularensis: taxonomy, genetics, and Immunopathogenesis of a potential agent of biowarfare. *Annu. Rev. Microbiol.* **60,** 167–185
6. Kingry, L. C., and Petersen, J. M. (2014) Comparative review of Francisella tularensis and Francisella novicida. *Front. Cell Infect. Microbiol.* **4,** 35
7. Brodmann, M., Dreier, R. F., Broz, P., and Basler, M. (2017) Francisella requires dynamic type VI secretion system and ClpB to deliver effectors for phagosomal escape. *Nat. Commun.* **8,** 15853
8. Eshraghi, A., Kim, J., Walls, A. C., Ledvina, H. E., Miller, C. N., Ramsey, K. M., Whitney, J. C., Radey, M. C., Peterson, S. B., Ruhland, B. R., Tran, B. Q., Goo, Y. A., Goodlett, D. R., Dove, S. L., Celli, J., Veesler, D., and Mougous, J. D. (2016) Secreted within and outside of the Francisella pathogenicity island promote intramacrophage growth. *Cell Host Microbe* **20,** 573–583
9. Lagrange, B., Benaoudia, S., Wallet, P., Magnotti, F., Provost, A., Michal, F., Martin, A., Di Lorenzo, F., Py, B. F., Molinaro, A., and Henry, T. (2018) Human caspase-4 detects tetra-acylated LPS and cytosolic Francisella and functions differently from murine caspase-11. *Nat. Commun.* **9,** 242
10. Santic, M., Molmeret, M., Klose, K. E., and Abu Kwaik, Y. (2006) Francisella tularensis travels a novel, twisted road within macrophages. *Trends Microbiol.* **14,** 37–44
11. Pizarro-Cerda, J., Charbit, A., Enninga, J., Lafont, F., and Cossart, P. (2016) Manipulation of host membranes by the bacterial pathogens Listeria, Francisella, Shigella and Yersinia. *Semin. Cell Dev. Biol.* **60,** 155–167.
12. Charity, J. C., Blalock, L. T., Costante-Hamm, M. M., Kasper, D. L., and Dove, S. L. (2009) Small molecule control of virulence gene expression in Francisella tularensis. *PLoS Pathog.* **5,** e1000641
13. Meibom, K. L., Barel, M., and Charbit, A. (2009) Loops and networks in control of Francisella tularensis virulence. *Future Microbiol.* **4,** 713–729
14. Celli, J., and Zahrt, T. C. (2013) Mechanisms of Francisella tularensis intracellular pathogenesis. *Cold Spring Harb. Perspect. Med.* **3,** a010314
15. Ramsey, K. M., Osborne, M. L., Vvedenskaya, I. O., Su, C., Nickels, B. E., and Dove, S. L. (2015) Ubiquitous promoter-localization of essential virulence regulators in Francisella tularensis. *PLoS Pathog.* 11, e1004793
16. Ziveri, J., Barel, M., and Charbit, A. (2017) Importance of metabolic adaptations in Francisella pathogenesis. *Front. Cell Infect. Microbiol.* **7,** 96
17. Bröms, J. E., Sjöstedt, A., and Lavander, M. (2010) The role of the Francisella Tularensis pathogenicity island in type VI secretion, intracellular survival, and modulation of host cell signaling. *Front. Microbiol.* **1,** 136
18. Clemens, D. L., Lee, B. Y., and Horwitz, M. A. (2018) The Francisella Type VI Secretion System. *Front. Cell Infect. Microbiol.* **8,** 121
19. Nano, F. E., Zhang, N., Cowley, S. C., Klose, K. E., Cheung, K. K., Roberts, M. J., Ludu, J. S., Letendre, G. W., Meierovics, A. I., Stephens, G., and Elkins, K. L. (2004) A Francisella tularensis pathogenicity island required for intramacrophage growth. *J. Bacteriol.* **186,** 6430–6436
20. Lauriano, C. M., Barker, J. R., Yoon, S. S., Nano, F. E., Arulanandam, B. P., Hassett, D. J., and Klose, K. E. (2004) MglA regulates transcription of virulence factors necessary for Francisella tularensis intraamoebae and intramacrophage survival. *Proc. Natl. Acad. Sci. U.S.A.* **101,** 4246–4249
21. Meyer, L., Broms, J. E., Liu, X., Rottenberg, M. E., and Sjostedt, A. (2015) Microinjection of Francisella tularensis and Listeria monocytogenes reveals the importance of bacterial and host factors for successful replication. *Infect. Immun.* **83,** 3233–3242
22. Cuthbert, B. J., Ross, W., Rohlfing, A. E., Dove, S. L., Gourse, R. L., Brennan, R. G., and Schumacher, M. A. (2017) Dissection of the molecular circuitry controlling virulence in Francisella tularensis. *Genes Dev.* **31,** 1549–1560
23. Russell, A. B., Wexler, A. G., Harding, B. N., Whitney, J. C., Bohn, A. J., Goo, Y. A., Tran, B. Q., Barry, N. A., Zheng, H., Peterson, S. B., Chou, S., Gonen, T., Goodlett, D. R., Goodman, A. L., and Mougous, J. D. (2014) A type VI secretion-related pathway in Bacteroidetes mediates interbacterial antagonism. *Cell Host Microbe* **16,** 227–236
24. Abby, S. S., Cury, J., Guglielmini, J., Neron, B., Touchon, M., and Rocha, E. P. (2016) Identification of protein secretion systems in bacterial genomes. *Sci. Rep.* **6,** 23080
25. Ledvina, H. E., Kelly, K. A., Eshraghi, A., Plemel, R. L., Peterson, S. B., Lee, B., Steele, S., Adler, M., Kawula, T. H., Merz, A. J., Skerrett, S. J., Celli, J., and Mougous, J. D. (2018) A phosphatidylinositol 3-kinase effector alters phagosomal maturation to promote intracellular growth of Francisella. *Cell Host Microbe* **24,** 285–295 e288
26. Clemens, D. L., Ge, P., Lee, B. Y., Horwitz, M. A., and Zhou, Z. H. (2015) Atomic structure of T6SS reveals interlaced array essential to function. *Cell* **160,** 940–951
27. Nazarov, S., Schneider, J. P., Brackmann, M., Goldie, K. N., Stahlberg, H., and Basler, M. (2018) Cryo-EM reconstruction of Type VI secretion system baseplate and sheath distal end. *EMBO J.* **37,** pii: e97103. doi: 10.15252/embj.201797103
28. Vettiger, A., and Basler, M. (2016) Type VI secretion system substrates are transferred and reused among sister cells. *Cell* **167,** 99–110 e112
29. Chamberlain, R. E. (1965) Evaluation of live Tularemia vaccine prepared in a chemically defined medium. *Appl. Microbiol.* **13,** 232–235
30. Gesbert, G., Ramond, E., Tros, F., Dairou, J., Frapy, E., Barel, M., and Charbit, A. (2015) Importance of branched-chain amino acid utilization in Francisella intracellular adaptation. *Infect. Immun.* **83,** 173–183
31. Lipecka, J., Chhuon, C., Bourderioux, M., Bessard, M. A., van Endert, P., Edelman, A., and Guerrera, I. C. (2016) Sensitivity of mass spectrometry analysis depends on the shape of the filtration unit used for filter aided sample preparation (FASP). *Proteomics* **16,** 1852–1857
32. Cox, J., and Mann, M. (2008) MaxQuant enables high peptide identification rates, individualized p.p.b.-range mass accuracies and proteome-wide protein quantification. *Nat Biotechnol* **26,** 1367–1372
33. Abd, H., Johansson, T., Golovliov, I., Sandstrom, G., and Forsman, M. (2003) Survival and growth of Francisella tularensis in Acanthamoeba castellanii. *Appl. Environ. Microbiol.* **69,** 600–606
34. Ziveri, J., Tros, F., Guerrera, I. C., Chhuon, C., Audry, M., Dupuis, M., Barel, M., Korniotis, S., Fillatreau, S., Gales, L., Cahoreau, E., and Charbit, A. (2017) The metabolic enzyme fructose-1,6-bisphosphate aldolase acts as a transcriptional regulator in pathogenic Francisella. *Nat. Commun.* **8,** 853
35. Rigard, M., Broms, J. E., Mosnier, A., Hologne, M., Martin, A., Lindgren, L., Punginelli, C., Lays, C., Walker, O., Charbit, A., Telouk, P., Conlan, W., Terradot, L., Sjostedt, A., and Henry, T. (2016) Francisella tularensis IglG belongs to a novel family of PAAR-like T6SS proteins and harbors a

unique N-terminal extension required for virulence. *PLoS Pathog.* **12,** e1005821
36. Meunier, E., Wallet, P., Dreier, R. F., Costanzo, S., Anton, L., Ruhl, S., Dussurgey, S., Dick, M. S., Kistner, A., Rigard, M., Degrandi, D., Pfeffer, K., Yamamoto, M., Henry, T., and Broz, P. (2015) Guanylate-binding proteins promote activation of the AIM2 inflammasome during infection with Francisella novicida. *Nat. Immunol.* **16,** 476–484
37. Edgar, R. C. (2004) MUSCLE: a multiple sequence alignment method with reduced time and space complexity. *BMC Bioinformatics* **5,** 113
38. Fu, A. Q., Genereux, D. P., Stoger, R., Burden, A. F., Laird, C. D., and Stephens, M. (2012) Statistical inference of in vivo properties of human DNA methyltransferases from double-stranded methylation patterns. *PLoS ONE* **7,** e32225
39. Robert, X., and Gouet, P. (2014) Deciphering key features in protein structures with the new ENDscript server. *Nucleic Acids Res.* **42,** W320–W324
40. Perez-Riverol, Y., Xu, Q. W., Wang, R., Uszkoreit, J., Griss, J., Sanchez, A., Reisinger, F., Csordas, A., Ternent, T., Del-Toro, N., Dianes, J. A., Eisenacher, M., Hermjakob, H., and Vizcaino, J. A. (2016) PRIDE inspector toolsuite: moving toward a universal visualization tool for proteomics data standard formats and quality assessment of ProteomeXchange datasets. *Mol. Cell. Proteomics* **15,** 305–317
41. Sullivan, J. T., Jeffery, E. F., Shannon, J. D., and Ramakrishnan, G. (2006) Characterization of the siderophore of Francisella tularensis and role of fslA in siderophore production. *J. Bacteriol.* **188,** 3785–3795
42. Kiss, K., Liu, W., Huntley, J. F., Norgard, M. V., and Hansen, E. J. (2008) Characterization of fig operon mutants of Francisella novicida U112. *FEMS Microbiol Lett.* **285,** 270–277
43. Roche, B., Aussel, L., Ezraty, B., Mandin, P., Py, B., and Barras, F. (2013) Reprint of: Iron/sulfur proteins biogenesis in prokaryotes: formation, regulation and diversity. *Biochim. Biophys. Acta* **1827,** 923–937
44. Mettert, E. L., and Kiley, P. J. (2015) Fe-S proteins that regulate gene expression. *Biochim. Biophys. Acta* **1853,** 1284–1293
45. Weiss, D. S., Brotcke, A., Henry, T., Margolis, J. J., Chan, K., and Monack, D. M. (2007) In vivo negative selection screen identifies genes required for Francisella virulence. *Proc. Natl. Acad. Sci. U.S.A.* **104,** 6037–6042
46. Broms, J. E., Lavander, M., and Sjostedt, A. (2009) A conserved alpha-helix essential for a type VI secretion-like system of Francisella tularensis. *J. Bacteriol.* **191,** 2431–2446
47. Spidlova, P., and Stulik, J. (2017) Francisella tularensis type VI secretion system comes of age. *Virulence* **8,** 628–631
48. Ramond, E., Gesbert, G., Guerrera, I. C., Chhuon, C., Dupuis, M., Rigard, M., Henry, T., Barel, M., and Charbit, A. (2015) Importance of host cell arginine uptake in Francisella phagosomal escape and ribosomal protein amounts. *Mol. Cell. Proteomics* **14,** 870–881
49. Wehrly, T. D., Chong, A., Virtaneva, K., Sturdevant, D. E., Child, R., Edwards, J. A., Brouwer, D., Nair, V., Fischer, E. R., Wicke, L., Curda, A. J., Kupko, J. J., 3rd, Martens, C., Crane, D. D., Bosio, C. M., Porcella, S. F., and Celli, J. (2009) Intracellular biology and virulence determinants of Francisella tularensis revealed by transcriptional profiling inside macrophages. *Cell Microbiol.* **11,** 1128–1150
50. Ludu, J. S., de Bruin, O. M., Duplantis, B. N., Schmerk, C. L., Chou, A. Y., Elkins, K. L., and Nano, F. E. (2008) The Francisella pathogenicity island protein PdpD is required for full virulence and associates with homologues of the type VI secretion system. *J. Bacteriol.* **190,** 4584–4595
51. Baroni, S., Pandini, V., Vanoni, M. A., and Aliverti, A. (2012) A single tyrosine hydroxyl group almost entirely controls the NADPH specificity of Plasmodium falciparum ferredoxin-NADP+ reductase. *Biochemistry* **51,** 3819–3826
52. Mougous, J. D., Gifford, C. A., Ramsdell, T. L., and Mekalanos, J. J. (2007) Threonine phosphorylation post-translationally regulates protein secretion in Pseudomonas aeruginosa. *Nat. Cell Biol.* **9,** 797–803
53. Silverman, J. M., Brunet, Y. R., Cascales, E., and Mougous, J. D. (2012) Structure and regulation of the type VI secretion system. *Annu. Rev. Microbiol.* **66,** 453–472
54. Cianfanelli, F. R., Monlezun, L., and Coulthurst, S. J. (2016) Aim, Load, Fire: The Type VI secretion system, a bacterial nanoweapon. *Trends Microbiol.* **24,** 51–62
55. Ostrowski, A., Cianfanelli, F. R., Porter, M., Mariano, G., Peltier, J., Wong, J. J., Swedlow, J. R., Trost, M., and Coulthurst, S. J. (2018) Killing with proficiency: Integrated post-translational regulation of an offensive Type VI secretion system. *PLoS Pathog.* **14,** e1007230
56. Aussel, L., Pierrel, F., Loiseau, L., Lombard, M., Fontecave, M., and Barras, F. (2014) Biosynthesis and physiology of coenzyme Q in bacteria. *Biochim. Biophys. Acta* **1837,** 1004–1011
57. van Hoek, M. L., Hoang, K. V., and Gunn, J. S. (2019) Two-component systems in Francisella species. *Front. Cell Infect. Microbiol.* **9,** 198
58. Nguyen, V. S., Douzi, B., Durand, E., Roussel, A., Cascales, E., and Cambillau, C. (2018) Towards a complete structural deciphering of Type VI secretion system. *Curr. Opin. Struct Biol.* **49,** 77–84